

**Functional and anatomical organization of
forward projection from area TE to perirhinal
neurons representing visual long-term
memory in monkeys.**

大脳側頭葉長期記憶ニューロンへの神経投射の放散度:生理学
的解剖学的手法による定量的解析

吉田 正俊

Table of Contents

Abstract	p. 03
Introduction	p. 04
Materials and Methods	p. 07
Results	p. 15
Discussion	p. 34
Acknowledgements	p. 38
References	p. 39

Abstract

A number of studies have shown that the perirhinal (PRh) cortex, which is part of the medial temporal lobe memory system, plays an important role in declarative long-term memory. The PRh cortex contains neurons that represent visual long-term memory. The aim of the present study is to characterize the anatomical organization of forward projections that mediate information flow from visual area TE to memory neurons in the PRh cortex. In monkeys performing a visual pair-association memory task, I conducted an extensive mapping of neuronal responses in anteroventral area TE (TEav) and area 36 (A36) of the PRh cortex. Then, three retrograde tracers were separately injected into A36 and the distribution of retrograde labels in TEav was analyzed. I focused on the degree of divergent projections from TEav to memory neurons in A36, because the highly divergent nature of these forward fiber projections has been implicated in memory function. I found that the degree of divergent projection to memory neurons in A36 was smaller from the TEav neurons selective to learned pictures than from the nonselective TEav neurons. This result demonstrates that the anatomical difference (the divergence) correlates with the physiological difference (selectivity of TEav neurons to the learned pictures). Because the physiological difference is attributed to whether or not the projections are involved in information transmission required for memory neurons in A36, it can be speculated that the reduced divergent projection resulted from acquisition of visual long-term memory, possibly through retraction of the projecting axon collaterals.

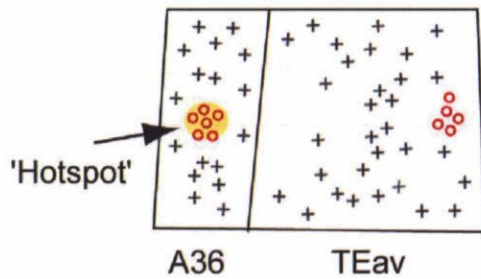
Introduction

It has been recognized that the perirhinal (PRh) cortex, which is part of the memory system in the medial temporal lobe (Squire and Zora-Morgan, 1991), plays a critical role in declarative long-term memory (Squire and Zora-Morgan, 1991; Miyashita, 1993). Lesions in the PRh cortex of macaque monkeys impair the formation of recognition memory (Zola-Morgan et al, 1989; Meunier et al., 1993) and stimulus-stimulus association memory (Murray, Gaffan and Mishkin, 1993). There is a double dissociation between the effects of lesion to the PRh cortex and those to area TE, which is a visual association cortex immediately adjacent to the PRh cortex (Buckley, Gaffan and Murray, 1997; Buffalo et al., 1999). Single-unit studies show that responses of PRh neurons represent visual associative long-term memory during (Messinger et al., 2001) and after learning (Sakai and Miyashita, 1991; Miyashita, 1988). Recently, we reported that the degree of memory-coding in PRh neurons was much higher than in TE neurons, which provided evidence that forward signal transmission from area TE to the PRh cortex is the critical step from visual to mnemonic processing, suggesting contributions of several long-term plasticity mechanisms for the critical step (Naya, Yoshida and Miyashita, 2003). In the present study, I sought an anatomical correlate of the plasticity mechanisms. The anteroventral part of area TE (TEav) sends dense and highly divergent fibers to area 36 (A36) of the PRh cortex (Suzuki and Amaral, 1994; Saleem and Tanaka, 1996). The highly divergent nature of this projection has been implicated in memory function (Suzuki and Amaral, 1994; Saleem and Tanaka, 1996). Thus, I focused on the degree of divergent projection from TEav to memory-related

neurons in A36.

The experimental design is illustrated in Fig. 1. In monkeys that were extensively trained in a visual pair-association memory task (Sakai and Miyashita, 1991; Higuchi and Miyashita, 1996), I recorded neuronal responses to learned pictures in A36 and TEav (Fig. 1, left). As expected from previous findings (Sakai and Miyashita, 1991; Miyashita, 1988; Naya, Yoshida and Miyashita, 2003), neurons selective to learned pictures were localized in a focal patch in A36 ('hotspot') (Fig. 1, left; see also Fig. 4) and they indeed coded visual long-term memory. Then, in a tracer injection study (Fig. 1, right), a retrograde tracer was injected into the hotspot ('hotspot injection') and two different kinds of tracer were injected as control ('control injection'). By combining anatomical and electrophysiological data, the degree of divergent projection from TEav neurons to the hotspot in A36 was compared between neurons involved (picture-selective neurons) and those not involved (nonselective neurons) in task-related visual processing (Fig. 1, right). Experiments were carefully designed to control the effect of the difference between monkeys using a within-animal comparison paradigm. The advantage of this experimental design is that it enhances the power to detect differences in anatomical measures as well as that it greatly reduces the problem arising from using different tracers.

Single-unit recording



Injection of retrograde tracers

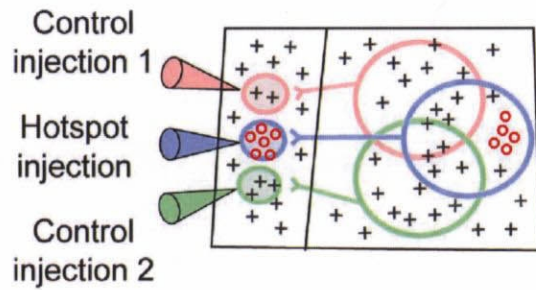


Fig. 1

The experimental design. (Left) I conducted an extensive mapping of neuronal responses in A36 and TEav. Recorded neurons were classified into picture-selective neurons (red circle) and nonselective neurons (gray cross). The picture-selective neurons in A36 were localized in the hotspot (yellow). (Right) Retrograde tracers were injected into the hotspot (hotspot injection) and adjacent control regions (control injection 1 and 2) in A36. Then, the distribution of retrograde labels in TEav was compared with the distribution of recorded neurons.

Materials and Methods

Behavioral task and electrophysiology.

All experiments were conducted in accordance with the NIH Guide for the Care and Use of Laboratory animals, U.S.A. and with the regulations of the National Institute for Physiological Sciences, Japan. Three adult monkeys (*Macaca fuscata*; 6.0 – 9.0 kg) were trained with a pair-association task using 24 monochrome Fourier descriptors (Fig. 2a) (Naya, Sakai and Miyashita, 1996; Naya Yoshida and Miyashita, 2001). The duration of experience that each animal had with the stimulus set before the beginning of recording sessions was 3.5 months in monkey A, 3 months in monkey B and 4 months in monkey C. The duration of recording in each animal was 12 months in monkey A, 10 months in monkey B and 14 months in monkey C. Single-unit recording was performed as described previously (Naya Yoshida and Miyashita, 2001). The three animals in the present study were also used in our previous electrophysiological study of IT cortex (Naya, Yoshida and Miyashita, 2003; Naya Yoshida and Miyashita, 2001). The recorded neurons in A36 and in TEav were classified as picture-selective or nonselective, based on the response during the cue period (60 – 320 ms after the cue onset, ANOVA, $P < 0.01$) (Naya Yoshida and Miyashita, 2001). The location of the electrode track for each recording session was measured on an X-ray image (Higuchi and Miyashita, 1996, Baylis, Rolls and Leonard, 1987). A potential source of error in estimation of the position of recorded neurons comes from the measurement of electrode positions on X-ray films. This was evaluated from the variance in the measurement of the distance between the external auditory meatus and the

posterior tip of the sphenoid bone (Aggleton and Passingham, 1981; Nishijo, Ono and Nishino, 1988; Nakamura, Mikami and Kubota, 1992) on the same X-ray film that recorded the electrode position in each recording session (28.16 ± 0.18 mm, mean \pm standard deviation). On construction of unfolded maps, additional information from anatomical geometry, for example, the shape of sulci and the thickness of gray matters, was used to estimate the position of recorded neurons. Thus, the error in the position on the map was estimated to be comparable to 0.18 mm standard deviation. Another independent measure for evaluating measurement error is the standard deviations of errors in the calibration of the positions of lesion marks and injection sites on the histological sections with those on X-ray films, which were 0.49, 0.35 and 0.20 mm for monkey A, B and C, respectively.

Triple injection and histology.

After the electrophysiological identification of the hotspot in A36, three different retrograde tracers (fast blue, FB, 3%, 150 – 180 nl; diamidino yellow, DY, 2%, 280 – 450 nl; cholera toxin B subunit, CTB, 10%, 100 nl) were injected separately into the hotspot and two control sites (Yoshida et al., 1999a, 1999b; Salin et al., 1992). The combination of injection sites and tracers in three monkeys was as follows: Monkey A: control 1, CTB; hotspot, FB; control 2, DY. Monkey B: control 1, DY; hotspot, FB; control 2, CTB. Monkey C: control 1, CTB; hotspot, FB; control 2, DY. The total numbers of retrograde labels in area TE were 19158, 16180 and 39205 (FB), 30160, 33641 and 14091 (DY) and 18699, 35478 and 23937 (CTB), in monkey A, B and C, respectively. There was no statistically significant difference in the number of retrograde labels between tracers ($F < 1$, repeated measures ANOVA). The

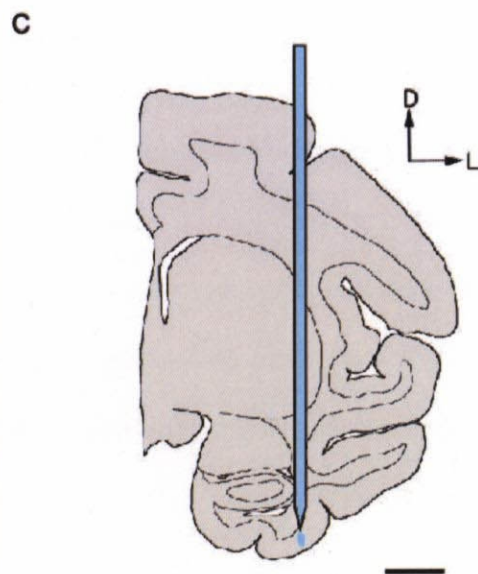
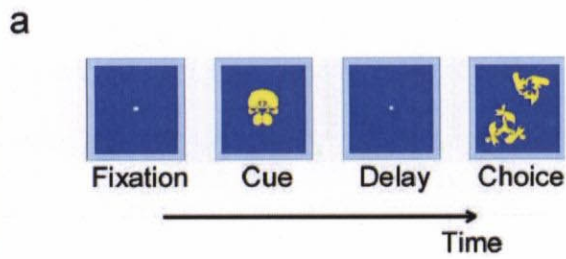


Fig. 2

Methods. (a) A sequence of the pair-association memory task. (b) and (c) The method of injection of retrograde tracers. (b) A glass micropipette containing a tungsten electrode. (c) The configuration of a glass micropipette during injection. rs, rhinal sulcus; amts, anterior middle temporal sulcus; sts, superior temporal sulcus. Scale bar, 0.5 mm, a; 5 mm, b. D, dorsal; L, lateral.

tracers were injected through a glass micropipette containing a tungsten electrode (Fig. 2b). The target location for injection was identified by recording neuronal activity with the electrode in the pipette (Fig. 2c) and by measuring the position of the electrode by X-ray imaging (Yoshida et al., 2000). This procedure enabled to confine the injected tracers to the gray matter of the target that was determined by the prior single-unit recording.

Fourteen days after the FB and DY injection and seven days after the CTB injection, the monkeys were perfused with 4% paraformaldehyde in phosphate buffer (pH 7.4). The brains were cut into 50 μm -thick coronal sections. One of every eight sections was used for data analysis. CTB was visualized by immunohistochemistry (Luppi, Fort and Jouvét, 1990). The position of neurons labeled by the retrograde tracers ('retrograde labels') was plotted with a computerized microscope system (KS400, Carl Zeiss Vision GmbH, Germany). The cytoarchitectonic borders were determined according to previous studies (Suzuki and Amaral, 1994; Saleem and Tanaka, 1996): There is a clear separation between layer 5 and layer 6 in TEav but not in A36. Layer 2 of A36 is thinner than that of TEav and contains patches of darkly stained cells. Layer 5 is less populated by neurons in TEad than in TEav. The extent of the tracers' uptake was determined according to the literature (Luppi, Fort and Jouvét, 1990; Conde, 1987).

Construction of two-dimensional unfolded map.

A flat map of retrograde labels was constructed according to a previous paper (Suzuki and Amaral, 1994). The gray matter was subdivided into rectangular regions ('pixels') along layer 4 with a width of 250 μm . The number of the retrograde labels was counted in each

pixel. The count was normalized by the area of the pixel and converted to a density value that was expressed as the number of labeled neurons per the average area of TE pixels. These procedures produced arrays of density values for each histological section. The arrays were then aligned section-by-section so that histological markers (e.g., border and sulcus) connected smoothly and so that the region of interest (either A36 in Fig. 4 or TEav in Fig. 6, 8 and 11) were aligned with the minimum distortion.

A flat map of single-unit recordings was constructed in the same manner as that of retrograde labels. The recording sites were histologically reconstructed from X-ray images (Higuchi and Miyashita, 1996; Naya Yoshida and Miyashita, 2001) based on 3 – 4 electrolytic lesions and three injected dyes. Shrinkage of histological sections (7 – 15 %) was corrected.

Data analysis.

The results of this study consist of four data sets: single-unit recording in A36 and in TEav, anatomy of A36 (tracer injection) and TEav (retrograde labels). The main purpose of data analysis is to compare the distribution of retrograde labels in TEav with that of single-unit recording in TEav.

A ‘hotspot’ was defined as a region with statistically significant percentage of picture-selective neurons, based on Kulldorff’s procedure (Kulldorff and Nagarwalla, 1995; Besag and Newell, 1991). This method is suitable for the present purpose in that it is applicable to sparsely sampled data, it does not assume spatial uniformity of sampling and it uses the number of sampled cells as the test statistics. This method uses a moving

window with a variable size and detects the window in which deviation of the percentage of picture-selective neurons from random samples is maximal, based on the binomial distribution. This analysis detected a small region where picture-selective neurons were significantly localized (2.0, 3.3 and 5.1 mm², $P < 0.001$, in each monkey). The defined hotspot contained 78 % (60 / 76) of picture-selective neurons in A36 (Yoshida, Naya and Miyashita, 2003). The correlation coefficient for paired pictures in the A36 picture-selective neurons that are not in the hotspot was significantly larger than zero (the median value = 0.45, $P = 0.006$, Wilcoxon signed-rank test; $n = 16$) and the median value was smaller than that of the picture-selective neurons in the A36 hotspot (0.52). The difference between the correlation coefficient of the A36 picture-selective neurons in the hotspot and that of neurons not in the hotspot was not significant ($P = 0.56$, Kolmogorov-Smirnov test), which may be due to the fact that the A36 picture-selective neurons that are not in the hotspot comprise a small population (16 / 76).

‘Clusters’ of retrograde labels were statistically defined in each map (three monkeys x three injections) as follows: If the retrograde labels were distributed randomly, the number of labeled neurons in each pixel should follow a Poisson distribution, $P(\lambda)$, where λ indicates the mean number of retrograde labels per pixel. The pixels were defined as a cluster when there were more than six contiguous pixels whose values were greater than the 95% level of distribution. Then, valleys on the two-dimensional maps were detected by image processing techniques (Haralick, 1983). Pixels defined as clusters but not separated from the injection site by valleys were excluded from the analysis.

In the region-of-interest (ROI)-based analysis, the percentage of picture-selective

neurons in each ROI was calculated using the equation: [number of picture-selective neurons in the ROI / {(number of picture-selective neurons in the ROI) + (number of nonselective neurons in the ROI)}] x 100. Their difference between ROIs was tested by the Cochran-Mantel-Haenszel (CMH) test (FREQ procedure in SAS) (Mantel and Haenszel, 1959), which is an extended version of χ^2 test. Its test statistics uses the number of counts of recorded neurons expressed as N_{ijk} , where i denotes whether they are picture-selective ($i = 1$) or not ($i = 2$), j denotes ROI ($j = 1,2$) and k denotes monkey ($k = 1-3$). The test statistics of CMH test, Q_{CMH} , is calculated as $(|\sum N_{11k} - \sum \{(N_{11k} + N_{21k}) * (N_{11k} + N_{12k}) / T_k\} - 0.5|^2 / \sum \{(N_{11k} + N_{21k}) * (N_{11k} + N_{12k}) * (N_{21k} + N_{22k}) * (N_{12k} + N_{22k}) / (T_k^2 * (T_k - 1))\})$, where $T_k = N_{11k} + N_{12k} + N_{21k} + N_{22k}$.

A map of the percentage of picture-selective neurons per pixel (Fig. 6, ‘Single-unit’ and Fig. 8b, middle) was constructed as follows. First, a map of the number of picture-selective neurons in each pixel and that of nonselective neurons in each pixel were constructed. Both maps were separately smoothed with a gaussian kernel ($\sigma = 500 \mu\text{m}$). A map of the percentage of picture-selective neurons per pixel was obtained as [the smoothed map of picture-selective neurons per pixel / {(the smoothed map of picture-selective neurons per pixel) + (the smoothed map of nonselective neurons per pixel)}] x 100.

‘Divergence index (DI)’ in each pixel on the map was defined as the ratio of the amount of projections to the hotspot injection site (y_2) to the total amount of projections to three injection sites ($y_1 + y_2 + y_3$) (Fig. 8a) (Yoshida et al., 2001a, 2001b). Note that when the DI analysis was made on the neurons in the cluster of HS retrograde labels, the density of HS retrograde labels (= y_2) in the analyzed pixels was always sufficiently larger than zero and

the denominator of DI ($= y_1 + y_2 + y_3$) can never be zero or near to zero. DI was also calculated with normalization in which the total number of retrograde labels was the same among the three tracers. The DI analysis is based on the distribution of labeled neurons on the equally spaced histological sections throughout area TE.

The statistical significance of the correlation coefficient was tested using a Monte Carlo simulation (Efron and Tibshirani, 1993). First, the data of recorded cells (in this case, whether the neuron is selective to pictures or not) was permuted within the cluster of HS retrograde labels of each monkey without changing the cells' spatial coordinates. Maps of the percentage of TEav picture-selective neurons per pixel were constructed in the same manner as that of the real data (Fig. 8b, middle). Then, the partial rank correlation coefficient between the permuted map of the percentage of picture-selective neurons (Fig. 8b, middle) and the DI map (Fig. 8b, left) was calculated. The distribution of correlation coefficient, which was predicted from the null hypothesis of no correlation, was constructed from 100,000 permutation data. P-value of the correlation coefficient of the real data was calculated from this distribution. It should be noted that it was not pixels but neurons that were permuted.

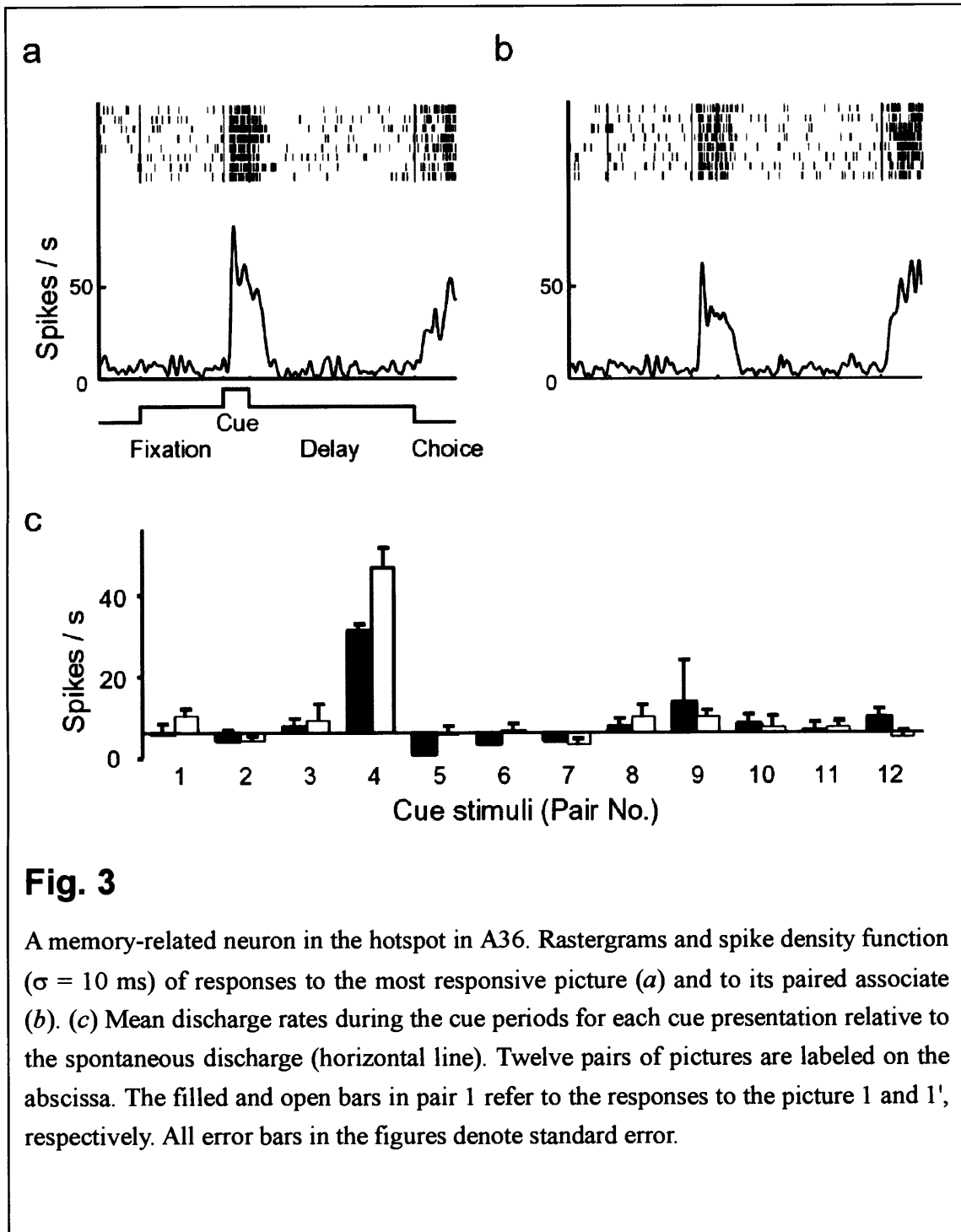
Results

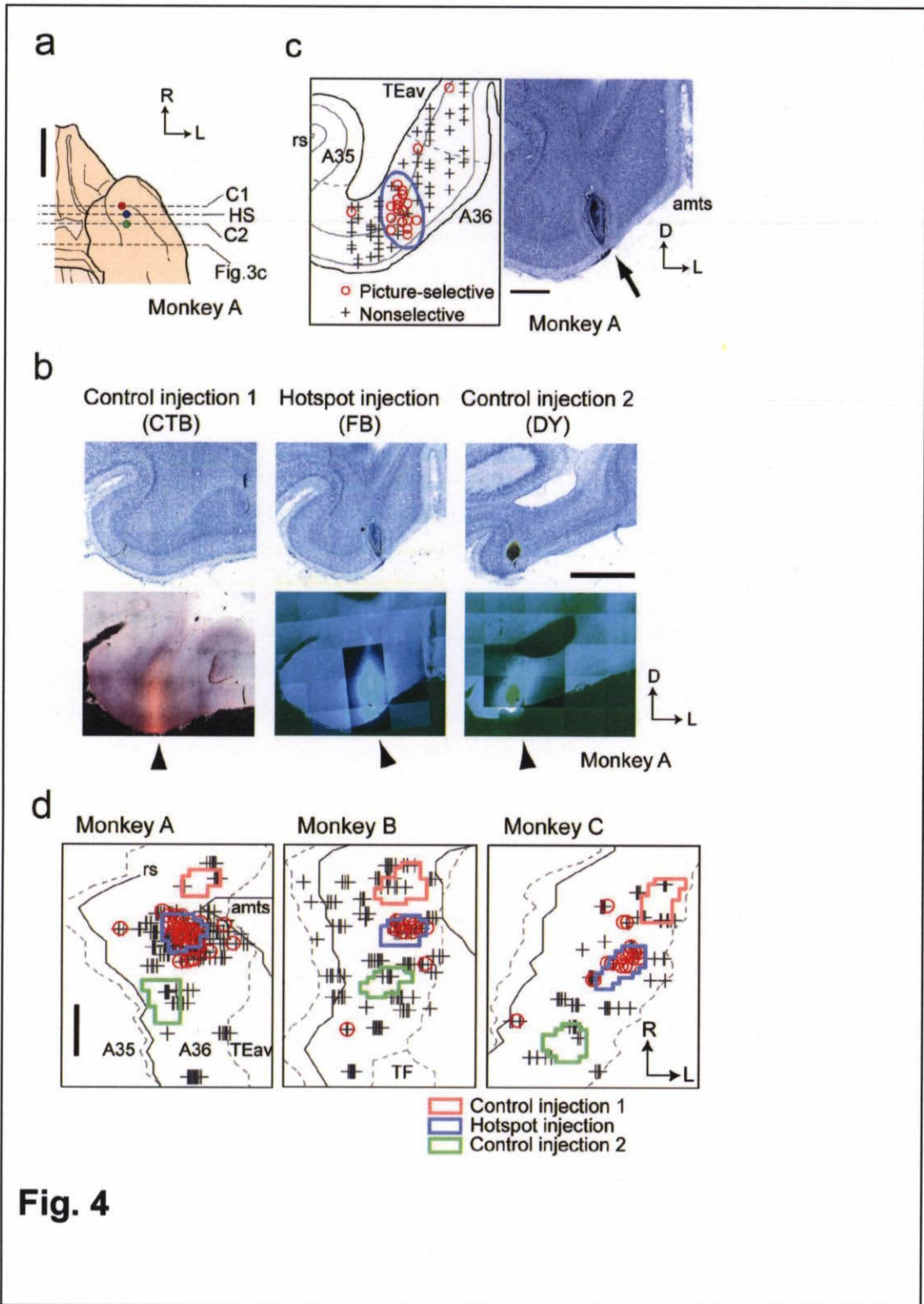
A ‘hotspot’ in A36.

In 510 neurons recorded in A36 of three monkeys, 85 were responsive and 76 showed selective response to the learned pictures during cue presentation (ANOVA, $P < 0.01$) (Naya, Yoshida and Miyashita, 2003). Figure 3 shows an example of picture-selective neurons in A36 that also showed preference for a pair of pictures (monkey A). The degree of memory coding was statistically significant in this neuron ($r = 0.92$, $P < 0.001$), quantified using the correlation coefficient between the cue responses to the paired pictures (Sakai and Miyashita, 1991; Higuchi and Miyashita, 1996). As demonstrated in a coronal section, A36 picture-selective neurons (red circle) were aggregated (Fig. 4c, left; monkey A). Two-dimensional unfolded maps of single-unit recording (Fig. 4d) revealed that most of A36 picture-selective neurons were localized in a focal patch (‘the hotspot’; See Methods) in each monkey. The degree of memory-coding in A36 hotspot, quantified using the correlation coefficient, was markedly larger than zero (median = 0.52, $P < 10^{-8}$, Wilcoxon signed-rank test; $n = 60$) (Naya, Yoshida and Miyashita, 2003). This result demonstrates that the picture-selective neurons in the A36 hotspot showed a strong memory-coding effect.

Triple injection of retrograde tracers into A36.

After the single-unit recording, three tracers (fast blue, FB; diamidino yellow, DY; cholera toxin B subunit, CTB) were injected into three regions in A36 (Fig. 4a and b). Injections





Legend

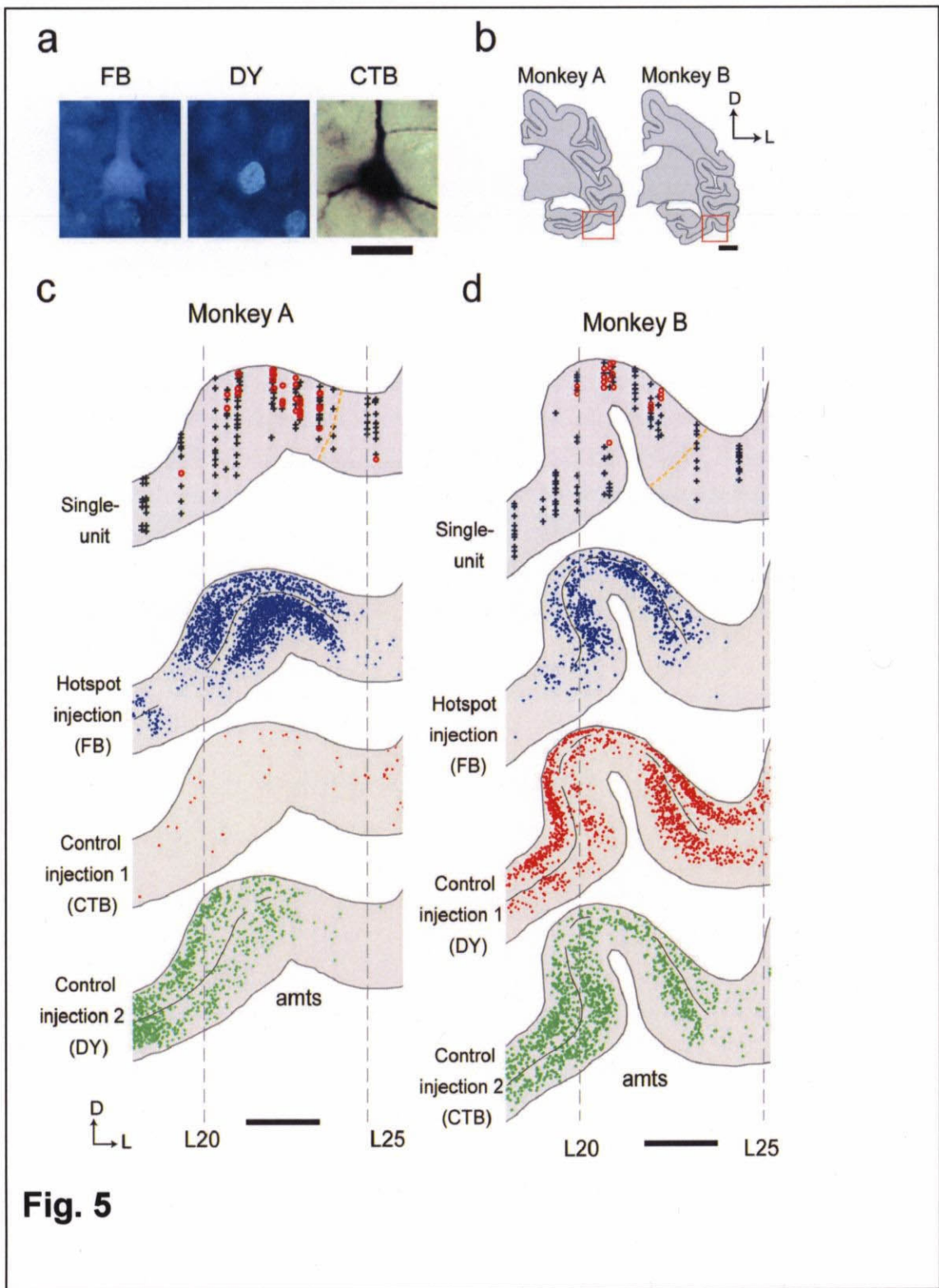
Fig. 4

Single-unit recording and tracer injection in A36. (a) Ventral view of a brain with an illustration of injection sites in A36. Circles show the locations of injection sites. Dotted lines denote the position of coronal sections containing injection sites displayed in *b* (HS, hotspot injection; C1 and C2, control injections) and the position of a section displayed in Fig. 5c. Monkey A. (b) Bright-field (top) and dark-field (lower) micrographs of coronal sections containing injection sites in A36. Arrowhead, injection site. The mosaic images were constructed by using a computerized microscope system. (c) A coronal section displaying the location of recorded neurons in A36 (left panel) and the corresponding Nissl section (right panel). Red circle, picture-selective neuron; gray cross, nonselective neuron; blue line, extent of the injection site; gray dotted line, border between A36 and TEav and border between A36 and A35. rs, rhinal sulcus; amts, anterior middle temporal sulcus. Arrow, injection site. (d) Extent of injection to the hotspot (blue) and control injections sites (red and green). Symbols are the same as *c*. Gray dotted line, border between A36 and adjacent areas; gray line, the lateral lip of rs (rs) and the medial lip of amts (amts). TF, area TF. Scale bars, 10 mm (*a*); 2 mm (*b* and *d*); 1 mm (*c*). R, rostral; L, lateral; D, dorsal.

were targeted to the hotspot and rostrocaudally adjacent control regions. Injection sites were clearly visible on the coronal sections as a core of each tracer with surrounding non-neuronal cells (Conde, 1987) after the injection of fluorescent tracers (arrowheads in Fig. 4b, middle and right) and as a homogeneously stained brown region (Luppi, Fort and Jouviet, 1990) after the injection of CTB (arrowhead in Fig. 4b, left). The identified injection site shows that the tracers were locally injected into the gray matter of A36 and that the tracers occupied most of the cortical layers (Fig. 4b and c). The unfolded maps demonstrate that the tracers were injected, as targeted, into the hotspot (Fig. 4d, 'hotspot injection') and the regions adjacent to but outside the hotspot (Fig. 4d, 'control injection 1 and 2'). The rostrocaudal diameter of the injection sites ranges 1.0 – 1.9 mm (mean 1.4 mm, $n = 9$). The distance between the center of the hotspot injection and the center of the control injection ranges 1.9 – 3.2 mm (mean 2.5 mm, $n = 6$).

Distribution of picture-selective neurons and retrograde labeling in TEav.

The distribution of recorded neurons and that of retrogradely labeled neurons were compared in TEav (Fig. 5). Out of 1189 recorded neurons in TEav, 262 were responsive and 232 were picture-selective (ANOVA, $P < 0.01$) (Naya, Yoshida and Miyashita, 2003). The correlation coefficient for paired pictures of the 232 neurons was significantly larger than zero (median = 0.14, $P < 0.001$, Wilcoxon signed-rank test) but much smaller than that of A36 picture-selective neurons (median value = 0.51; $P < 10^{-6}$; Kolmogorov-Smirnov test) (Naya, Yoshida and Miyashita, 2003). Retrogradely labeled neurons in TEav (FB, DY and CTB) are shown in Fig. 5a. The distribution of retrogradely labeled neurons and



Legend

Fig. 5

Single-unit recording and retrograde labels in TEav. (a) Retrogradely labeled neurons in TEav. (b) Coronal sections including recording sites in TEav. Red rectangles denote the regions displayed in *c* and *d*. (c) and (d) The location of recorded neurons (top panel) and the distribution of retrograde labels (lower three panels) in TEav of monkey A (*c*) and monkey B (*d*). In the single-unit recording display, data from four slices (~1.6 mm) were superimposed. Symbols are the same as Fig. 3c. In the retrograde labels display, data from two slices (~0.8 mm) were superimposed. Each dot denotes a single retrogradely labeled neuron. Black lines in the depth of the layer IV denote the regions included as clusters. Note that the threshold for clusters was different between subjects and tracers. Gray dotted lines denote coordinates determined from X-ray imaging. L20, for example, denotes the line 20 mm lateral to the center. Orange dotted line, border between TEav and TEad. Scales, 50 μm (A); 5 mm (B); 2 mm, (C) and (D). L, lateral; D, dorsal.

recorded neurons of two monkeys is shown in Fig. 5c and d. TEav picture-selective neurons (red circles) were localized around the anterior middle temporal sulcus (Fig. 5c and d, top panels). The distribution of retrograde labels at the same rostrocaudal level is also shown (Fig. 5c and d, bottom panels). Neurons retrogradely labeled by the hotspot injection ('HS retrograde labels') and those labeled by the control injections ('C1 or C2 retrograde labels') aggregated around the anterior middle temporal sulcus, forming 'clusters' of labels (Fig. 5c and d). The clusters from different tracers were not segregated but partially overlapped. A comparison of the single-unit (Fig. 5c and d, top panels) and retrograde labels (Fig. 5c and d, lower panels) revealed (i) that the regions in which TEav picture-selective neurons aggregated are included in the cluster of HS retrograde labels. The comparison also shows (ii) that within the cluster of HS retrograde labels, the regions with sparse C1 or C2 retrograde labels contained abundant picture-selective neurons in TEav.

To further quantify the above observations (i and ii), I compared two-dimensional unfolded maps of the density of retrograde labels in TEav (Fig. 6, 'Retrograde label') with that of single-unit recording (Fig. 6, 'Single-unit') (Naya, Yoshida and Miyashita, 2003). The regions densely labeled by the tracer were defined statistically as 'clusters' in each retrograde label map (See Methods). In each of three retrograde label maps, two or three clusters were detected in TEav (Fig. 6, 'Retrograde label', white line). Densely labeled regions around the injection sites (Fig. 6, 'Retrograde label', purple line) were excluded from the analysis. The observation (i) was statistically tested by the region-of-interest (ROI)-based analysis (see Methods): In each ROI (for example, the cluster of HS retrograde labels), the percentage of TEav picture-selective neurons was calculated. The percentage of

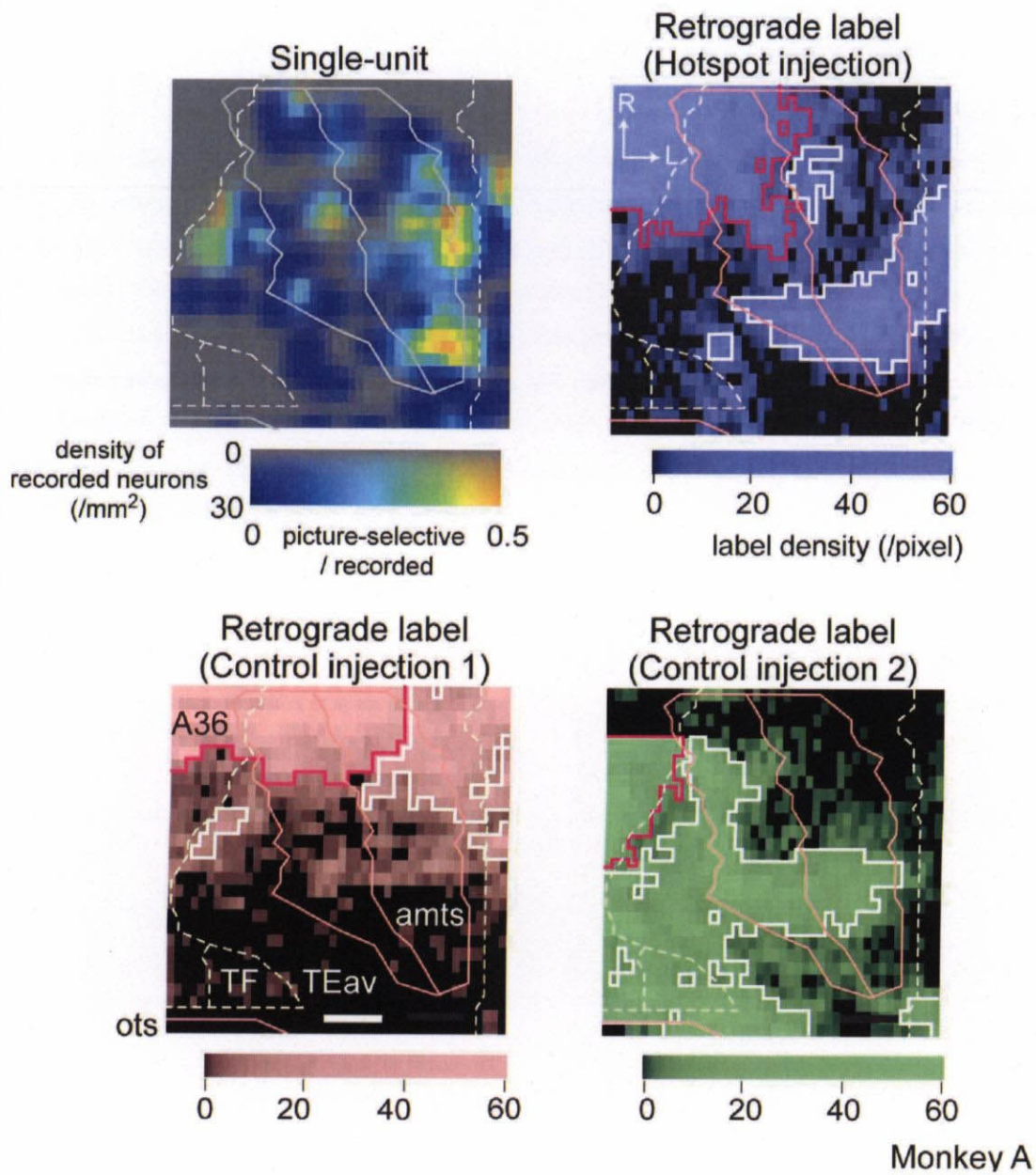


Fig. 6

Legend

Fig. 6

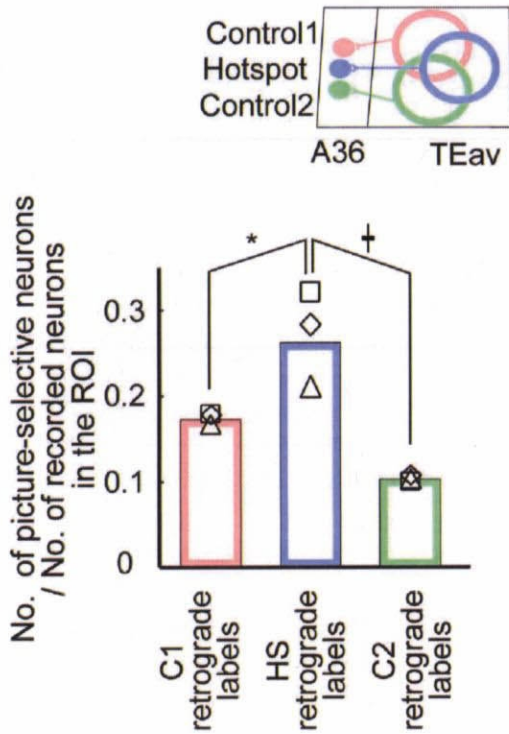
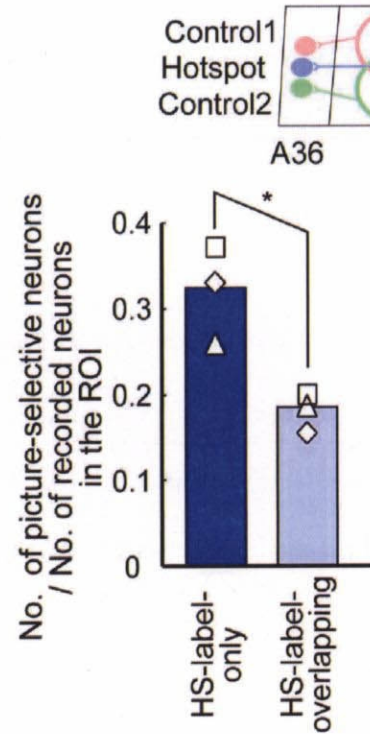
A comparison of the distribution of retrogradely labeled neurons in TEav with that of picture-selective neurons. Two-dimensional unfolded maps of single-unit and retrograde labels (hotspot injection, control injection 1 and 2) are displayed. In the single-unit map, the saturation of the colorbar denotes the density of recorded neurons and the hue denotes the number of picture-selective neurons per pixel / the number of recorded neurons per pixel. In retrograde label maps, the density of retrograde labels is color-coded. White line, pixels defined as clusters; purple line, densely labeled pixels near the injection site (see Methods). Borders and sulci are shown in lines. Monkey A. Scale bars, 2 mm. R, rostral; L, lateral.

TEav picture-selective neurons inside the clusters of the HS retrograde labels was significantly higher than that inside the clusters of the C1 or C2 retrograde labels in three monkeys ($\chi^2_1 = 9.0$, $P = 0.003$, HS retrograde labels vs. C1 retrograde labels; $\chi^2_1 = 40.7$, $P < 0.001$, HS retrograde labels vs. C2 retrograde labels; CMH test; Fig. 7a). This result confirmed the observation (i) and demonstrated that the clusters of HS retrograde labels in TEav preferentially provide the task-related visual information to the hotspot in A36.

Next, I tested the observation (ii) statistically. For this purpose, the clusters of HS retrograde labels were subdivided into two regions according to whether the region is included within the clusters of C1 or C2 retrograde labels ('HS-label-overlapping') or not ('HS-label-only') (Fig. 7b). The percentage of TEav picture-selective neurons was significantly higher in the 'HS-label-only' region than in the 'HS-label-overlapping' region ($\chi^2_1 = 11.5$, $P < 0.001$; CMH test; Fig. 7b), confirming the observation (ii).

Fine structure within clusters of HS retrograde labels.

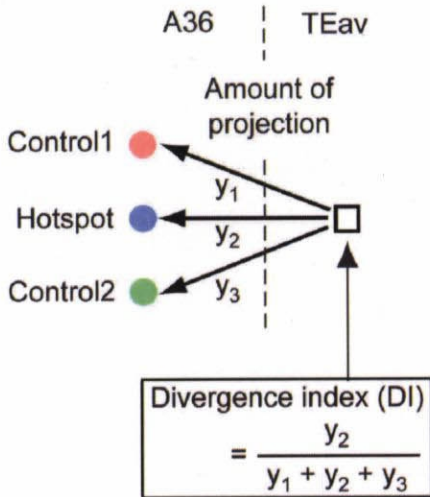
The result in Fig. 7b demonstrates that the 'HS-label-only' region contains more abundant TEav picture-selective neurons than the 'HS-label-overlapping' region does. By definition, the 'HS-label-only' region projects less divergently to the hotspot in A36 than does the 'HS-label-overlapping' region. Thus, these two lines of evidence indicate that the region containing abundant TEav picture-selective neurons ('HS-label-only' region) projects less divergently to the hotspot in A36. This finding raises a possibility that the TEav picture-selective neurons themselves project less divergently to the hotspot than do the TEav nonselective neurons. In order to test this possibility, I compared the degree of

a**b****Legend****Fig. 7**

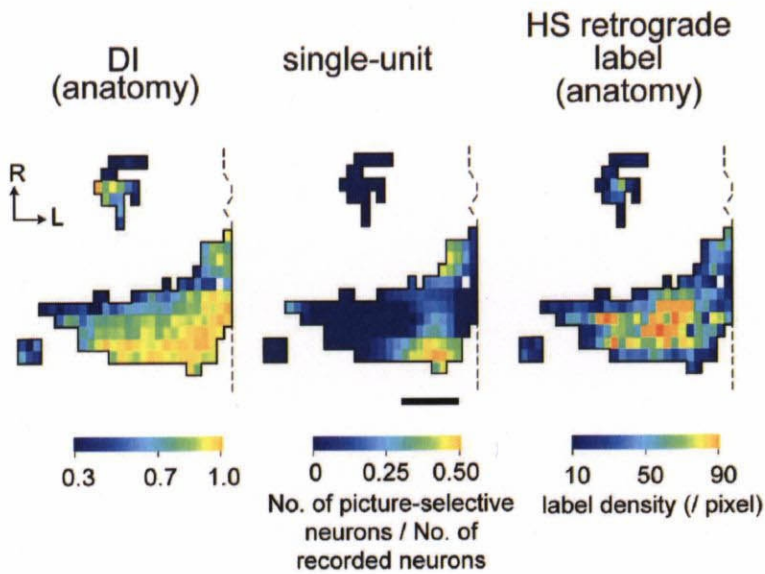
A comparison of the distribution of picture-selective neurons between ROIs. (a) and (b) the number of picture-selective neurons in the ROI / the number of recorded neurons in the ROI. In a, the ROIs are clusters of the C1 retrograde labels, the HS retrograde labels and the C2 retrograde labels, respectively. In b, the ROIs are the region outside ('HS-label-only') and inside ('HS-label-overlapping') the clusters of C1 or C2 retrograde labels. Each symbol denotes the value of each monkey (diamond, monkey A; square, monkey B; triangle, monkey C). *, $P < 0.005$; †, $P < 0.001$ in (a). *, $P < 0.001$ in (b).

divergent projection between TEav picture-selective and TEav nonselective neurons by defining 'divergence index (DI)' (Fig. 8a and Methods). If DI of a pixel is high, then neurons in the pixel project less divergently to the hotspot injection site. A correlation analysis based on Monte Carlo technique (See Methods for further detail) demonstrated that the map of the percentage of TEav picture-selective neurons (Fig. 8b, middle) was spatially correlated with the DI map (Fig. 8b, left) ($r = 0.38$, $P < 0.05$). In other two monkeys, the maps were also spatially correlated ($r = 0.30$ and 0.17 , $P < 0.05$ in both monkeys).

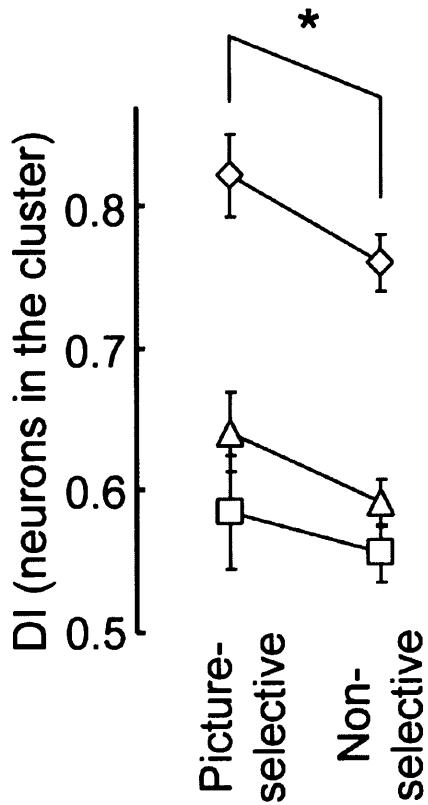
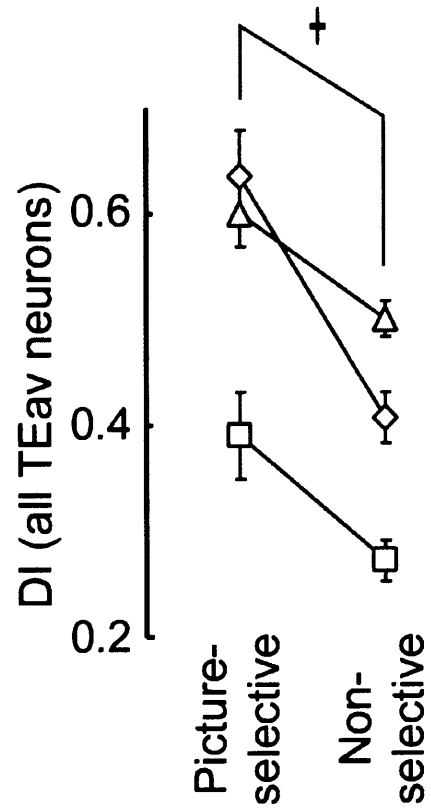
These observations were further confirmed by an analysis on a neuron-by-neuron basis: I assigned to each recorded neuron the DI that was linearly interpolated from DIs in the surrounding pixels and then the DI was compared between TEav picture-selective neurons and nonselective neurons (Fig. 9a). Two-way ANOVA [monkey x neuron type] indicated that DI was significantly higher in TEav picture-selective neurons than in TEav nonselective neurons ($F_{1, 505} = 6.05$, $P = 0.014$, after logit conversion; Fig. 9a). There was no significant interaction between monkey and neuron type ($F_{2, 505} = 0.45$, $P = 0.63$). When the difference in the total number of retrograde labels was normalized (see Methods), the result also showed statistical significance ($F_{1, 505} = 6.39$, $P = 0.011$, after logit conversion) and the interaction between monkey and neuron type was not significant ($F_{2, 505} = 0.48$, $P = 0.62$). When the ANOVA was performed with all recorded TEav neurons, the result was the same as that for neurons inside the cluster ($F_{1, 927} = 37.09$, $P < 0.001$, after logit conversion; Fig. 9b). All of these results indicate that picture-selective neurons in TEav project less divergently to the hotspot injection site than do nonselective neurons in TEav.

a**Fig. 8**

Divergence index (DI). (a) Calculation of DI. Amount of the projection from neurons in a TEav pixel (right square) to three injection sites (left circles) is expressed as y_1 , y_2 and y_3 (control injection 1, hotspot injection and control injection 2, respectively). DI was defined as $y_2 / (y_1 + y_2 + y_3)$.

b

(b) A map of DI (left), a single-unit map (middle) and a map of the density of HS retrograde labels (right). Color bars show the value of each pixel. Monkey A. Scale bar, 2 mm. R, rostral; L, lateral.

a**b****Fig. 9**

Comparison of DI between picture-selective neurons and nonselective neurons. DI of TEav neurons in the cluster of HS retrograde labels (*a*) and of all recorded TEav neurons (*b*) were compared between picture-selective neurons and nonselective neurons. The mean value and standard error for each monkey is expressed as symbols and error bars. The symbols denote the same as Fig. 7a. *, $P < 0.02$. †, $P < 0.001$.

Because $DI (= y_2 / (y_1 + y_2 + y_3))$ is a function of the density of HS retrograde labels ($= y_2$), I examined a possibility that the high DI in the TEav picture-selective neurons (Fig. 9a) might simply reflect a high density of HS retrograde labels. However, a comparison of maps indicates that the pixels with the highest percentage of TEav picture-selective neurons (Fig. 8b, middle) did not coincide with the pixels with the highest density of HS retrograde labels (Fig. 8b, right). These two maps were not spatially correlated ($r = 0.04, -0.11$ and -0.02 , in three monkeys). Moreover, two-way ANOVA indicated that the density of HS retrograde labels was not higher in TEav picture-selective neurons than in TEav nonselective neurons (See Legend of Fig. 10 for further details). Thus, the above possibility was rejected. It should be also noted that a scheme that the response property of A36 neurons were solely determined by a simple summation of input from TEav and by a global topographical pattern of connectivity from TEav to A36 will predict that the regions with the highest percentage of picture-selective neurons coincide with the regions with the highest density of HS retrograde labels. Because this was not the case (Fig. 8b, middle and right), the above scheme cannot explain my results.

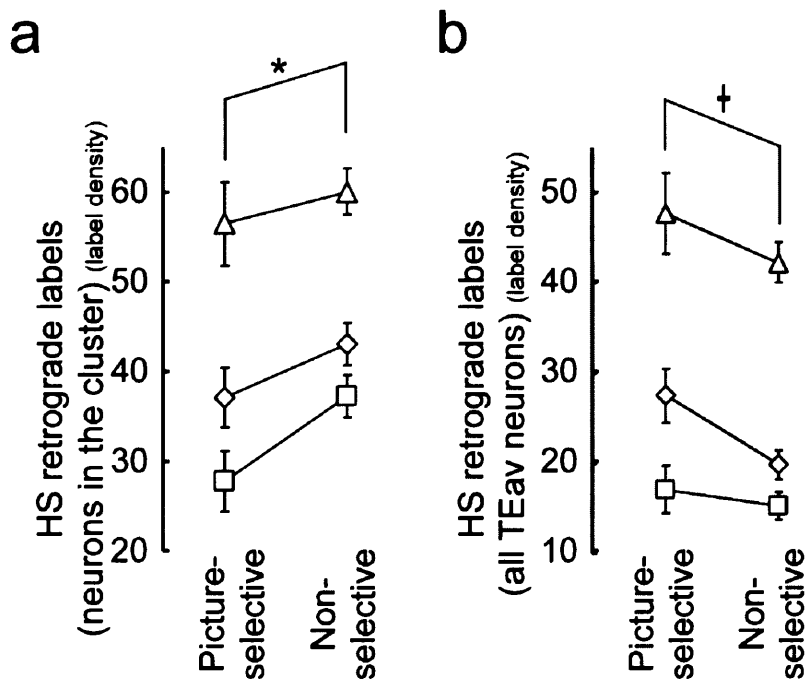


Fig. 10

The density of HS retrograde labels of TEav neurons in the cluster of HS retrograde labels (a) and of all recorded TEav neurons (b) was compared between picture-selective neurons and nonselective neurons. The mean value and standard error for each monkey is expressed as symbols and error bars. Each symbol denotes the value of each monkey (diamond, monkey A; square, monkey B; triangle, monkey C). In (a), the density of HS retrograde labels was not higher, actually it was significantly lower ($F_{1, 505} = 5.51$, $P = 0.019$, after logarithmic conversion, two-way ANOVA), in TEav picture-selective neurons than in TEav nonselective neurons. There was no significant interaction between monkey and neuron type ($F_{2, 505} = 1.45$, $P = 0.23$). Note that the result in (a) does not contradict the result shown in Fig. 7a: When the same analysis was performed on the population of all TEav neurons including inside and outside of the cluster of HS retrograde labels (b), the result showed that the density of HS retrograde labels was significantly higher for picture-selective neurons than for nonselective neurons ($F_{1, 929}$, $P < 0.001$). *, $P < 0.02$. †, $P < 0.001$.

Distribution of double-labeled (DL) neurons.

The distribution of neurons labeled with both FB and DY (double-labeled (DL) neurons) directly indicates the distribution of TEav neurons projecting divergently to both the hotspot and the control injection sites. The DL neurons (neurons labeled with both FB and DY) were readily distinguished from the neurons labeled only by FB or DY, by having a bright yellowish green nucleus in light-blue cytoplasm (Fig. 11a, DL). In three monkeys, most of the DL neurons (790 / 892, 89 %) were found in the clusters of HS retrograde labels. The unfolded map demonstrates that the aggregates of DL neurons (Fig. 11b, black circle) were segregated from the pixels where the picture-selective neurons were dense (Fig. 11b, red circle; for clarity, nonselective neurons were not displayed). This observation was quantified by subdividing the clusters of HS retrograde labels into pixels with DL neurons (DL+) and pixels without DL neurons (DL-). The percentage of picture-selective neurons was significantly smaller in the DL+ region than in the DL- region ($\chi^2_1 = 21.0$, $P < 0.001$, CMH test; Fig. 11c). This result suggests that the picture-selective neurons have less divergent projection to the hotspot injection site than do the nonselective neurons. Thus, the analysis of DL neurons provided further evidence that picture-selective neurons in TEav project less divergently to the hotspot injection site. This finding further clarifies the results of the analysis using divergence index (DI): In the analysis of DI (Fig. 9a), the projection from a pixel can be divergent either when axons of neurons in the pixel actually bifurcate or when different neurons in the pixel project to different targets. The analysis of DL neurons suggests that the latter possibility is unlikely.

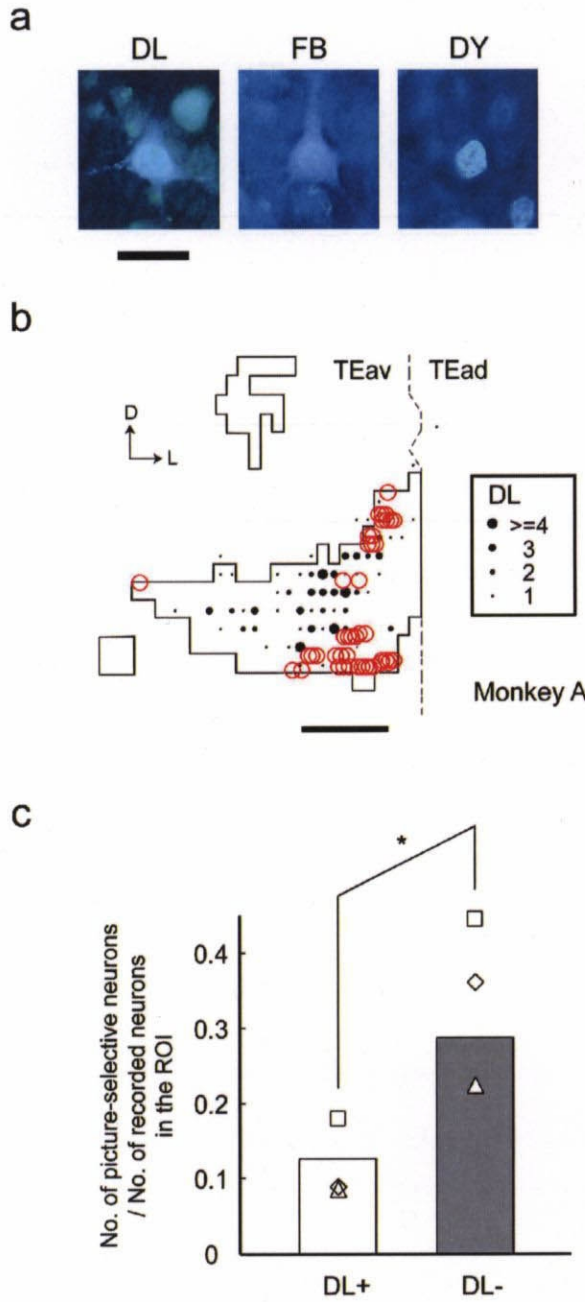


Fig. 11

Spatial relation between the distribution of picture-selective neurons and double-labeled (DL) neurons. (a) A DL neuron in TEav. For comparison, neurons labeled by FB or DY are also displayed. (b) A two-dimensional unfolded map showing the distribution of picture-selective neurons (red circle) and DL neurons (black circle) within the cluster of HS retrograde labels (lines) in TEav. For clarity, the distribution of nonselective neurons was not displayed. Each red circle denotes a single picture-selective neuron. Number of DL neurons in each pixel is expressed as the size of the circle. DL neurons outside the cluster are also shown. Most of DL neurons were found in the cluster of HS retrograde labels (104 / 110, 95 %). Monkey A. (c) The number of picture-selective neurons / the number of recorded neurons is compared between the pixels with (DL+) and without (DL-) DL neurons. The symbols denote the same as Fig. 7a. *, $P < 0.001$. †, $P < 0.001$.

Discussion

In this study, I trained monkeys to learn the pair-association memory task and characterized the connectivity that provides visual information from TEav to memory-coding neurons in A36. I found that TEav neurons selective to learned pictures project less divergently to the hotspot injection site in A36 where memory-coding neurons aggregate, than do nonselective neurons in TEav (Fig. 9 and 11). This result demonstrates that the morphological difference, that is, the difference in the degree of divergent projection, is coupled to the physiological difference between neurons selective to learned pictures and nonselective neurons. Both the selective and nonselective neurons share similar properties in that they project to the hotspot injection site and that they likely provide visual information to the hotspot in A36 (see the next paragraph). Thus, the physiological difference between these neurons indicates whether or not these neurons participate in the transmission of task-related visual information to the hotspot in A36. Therefore, I conclude that the morphological difference is coupled to the involvement of task-related visual processing. The present study demonstrates that this coincidence between the morphological difference and the physiological difference is found consistently among all monkeys.

A potential caveat for the above discussion is that neurons selective to learned pictures and nonselective neurons may differ in physiological aspects other than their involvement in task-related visual processing. However, although most of the TEav neurons classified as 'nonselective' were unresponsive to the learned pictures, these neurons are likely to be

visually responsive. The visual responsiveness of TEav neurons is well established from previous studies. Anatomically, TEav is a unimodal association cortex (Squire and Zora-Morgan, 1991; Miyashita, 1993). Baylis et. al. (Baylis, Rolls and Leonard, 1987) showed in a single-unit study that TEav neurons are exclusively responsive to visual stimuli. Tamura and Tanaka (Tamura and Tanaka, 2001) reported that at least 79 % of neurons recorded in TEav are responsive to object images. Thus, the physiological difference between selective and nonselective neurons lies in whether they are involved in task-related visual processing or not.

Observations in the present retrograde labeling study are consistent with those in previous anatomical studies. Strong connections from TEav to A36 have been reported (Suzuki and Amaral, 1994; Saleem and Tanaka, 1996). The partial overlap of retrograde labels for different tracers (Fig. 5 and 6) is consistent with previous reports on the divergent projection from TEav to A36 (Suzuki and Amaral, 1994; Saleem and Tanaka, 1996). One novel finding in the present study is that the TEav region with dense picture-selective neurons project specifically to the A36 region where memory-coding neurons were localized (Fig. 7a).

Previous electrophysiological studies demonstrate that structures similar to the hotspot emerge as a result of behavioral learning or experience (Sakai and Miyashita, 1991; Miyashita, 1988; Naya, Yoshida and Miyashita, 2003; Erickson, Jagadeesh and Desimone, 2000). BDNF mRNA is selectively induced in a focal patch within A36 during memory formation (Tokuyama et al., 2000). Lesion studies demonstrated a functional double dissociation that the PRh cortex is engaged in a mnemonic processing while area TE is

devoted to a perceptual processing (Buckley, Gaffan and Murray, 1997; Buffalo et al., 1999). Recently, we have found in a single-unit study that association between the representations of paired associates proceeds forward from TE to A36 (Naya, Yoshida and Miyashita, 2003), which is consistent with the above lesion studies. The results of the present study, together with those of the above studies, support the view that forward signal transmission from area TE to A36 is the critical step from visual to mnemonic processing.

Considering all of the findings in this study, I speculate that the reduced divergent projection may be the result of the acquisition of visual long-term memory. One of possible schemes is that, after extensive visual learning, fiber terminals projecting outside the hotspot retract in TEav neurons selective to learned pictures while fiber terminals of nonselective neurons retain their divergence (Fig. 12). Retraction of axon collaterals has been reported in development of the primary visual cortex (Antonini and Stryker, 1993; Borrell and Callaway, 2002). Cortical map reorganization induced by lesions in adulthood (Darian-Smith and Gilbert, 1994; Buonomano and Merzenich, 1998; Sur and Leamey, 2001) accompanies newly sprouted afferent terminals. Thus, the reduced divergent projection after learning found in the present study may share common mechanisms with cortical reorganization during development and/or regeneration.

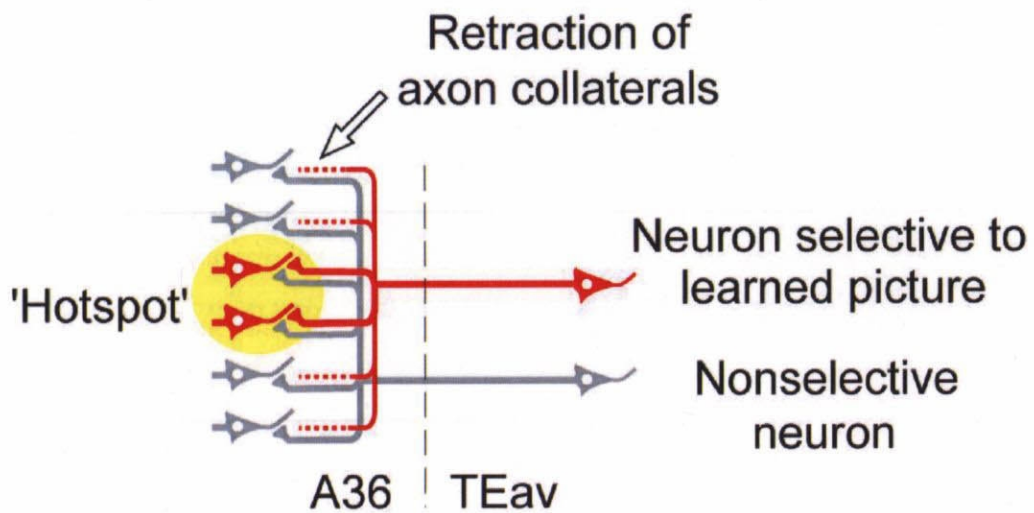


Fig. 12

A proposed scheme explaining the morphological basis of the reduced divergent projection found in this study. After extensive visual learning, fiber terminals projecting outside the hotspot were retracted in neurons selective to learned pictures (red). On the other hand, fiber terminals of nonselective neurons (gray) retained their divergence. Yellow circle denotes the hotspot in A36.

Acknowledgements

I am sincerely grateful to Professor Yasushi Miyashita for supervision and continuous supports during the course of this study. I thank Yuji Naya, Akimitsu Ito and Shuko Shibata for support in the experiments. I also thank Kenichi Ohki, Hiroyuki Okuno, Kiyoshi Nakahara, Masao Yukie, Yasushi Kobayashi, Tadashi Isa, Minami Ito, Hidehiko Komatsu, Kiyoji Matsuyama, and Shigemi Mori for discussions and comments. I am grateful to Professor Hiroshi Saito and Professor Norio Matsuki for encouragements.

References

- Aggleton, J.P., & Passingham, R.E. (1981) Stereotaxic surgery under X-ray guidance in the rhesus monkey, with special reference to the amygdala. *Exp. Brain Res.* **44**, 271-276.
- Antonini, A., & Stryker, M.P. (1993) Rapid remodeling of axonal arbors in the visual cortex. *Science* **260**, 1819-1821.
- Baylis, G.C., Rolls, E.T., & Leonard, C.M. (1987) Functional subdivisions of the temporal lobe neocortex. *J. Neurosci.* **7**, 330-342.
- Besag, J., & Newell, J. (1991) The detection of clusters in rare diseases. *J. Roy. Stat. Soc. A* **154**, 143-155
- Borrell, V., & Callaway, E.M. (2002) Reorganization of exuberant axonal arbors contributes to the development of laminar specificity in ferret visual cortex. *J. Neurosci.* **22**, 6682-6695.
- Buckley, M.J., Gaffan, D., and Murray, E. A. (1997) Functional double dissociation between two inferior temporal cortical areas: perirhinal cortex versus middle temporal gyrus. *J. Neurophysiol.* **77**, 587-598.
- Buffalo, E.A., Ramus, S.J., Clark, R.E., Teng, E., Squire, L.R., & Zola, S.M. (1999) Dissociation between the effects of damage to perirhinal cortex and area TE. *Learn. Mem.* **6**, 572-599.
- Buonomano, D.V., & Merzenich, M.M. (1998) Cortical plasticity: from synapses to maps. *Annu. Rev. Neurosci.* **21**, 149-186.
- Conde, F. (1987) Further studies on the use of the fluorescent tracers fast blue and

- diamidino yellow: effective uptake area and cellular storage sites. *J. Neurosci. Methods* **21**, 31-43.
- Darian-Smith, C., & Gilbert, C.D. (1994) Axonal sprouting accompanies functional reorganization in adult cat striate cortex. *Nature* **368**, 737-740.
- Efron, B., & Tibshirani, R. (1993) *An Introduction to the Bootstrap*. (Chapman and Hall, New York).
- Erickson, C.A., Jagadeesh, B., & Desimone, R. (2000) Clustering of perirhinal neurons with similar properties following visual experience in adult monkeys. *Nat. Neurosci.* **3**, 1143-1148.
- Haralick, R.M. (1983) Ridges and valleys on digital images. *Comput. Vision Graph. Image Process.* **22**, 28-38.
- Higuchi, S., & Miyashita, Y. (1996) Formation of mnemonic neuronal responses to visual paired associates in inferotemporal cortex is impaired by perirhinal and entorhinal lesions. *Proc. Natl. Acad. Sci. U.S.A.* **93**, 739-743.
- Kulldorff, M., & Nagarwalla, N. (1995) Spatial disease clusters: detection and inference. *Stat. Med.* **14**, 799-810.
- Luppi, P.H., Fort, P., & Jouviet, M. (1990) Iontophoretic application of unconjugated cholera toxin B subunit (CTb) combined with immunohistochemistry of neurochemical substances: a method for transmitter identification of retrogradely labeled neurons. *Brain Res.* **534**, 209-224.
- Mantel, N., & Haenszel, W. (1959) Statistical Aspects of the Analysis of Data from Retrospective Studies of Disease. *J. Nat'l. Canc. Inst.* **22**, 719 -748.

- Messinger, A., Squire, L.R., Zola, S.M., & Albright, T.D. (2001) Neuronal representations of stimulus associations develop in the temporal lobe during learning. *Proc. Natl. Acad. Sci. U.S.A.* **98**, 12239-12244.
- Meunier, M., Bachevalier, J., Mishkin, M., & Murray, E.A. (1993) Effects on visual recognition of combined and separate ablations of the entorhinal and perirhinal cortex in rhesus monkeys. *J. Neurosci.* **13**, 5418-5432.
- Miyashita, Y. (1988) Neuronal correlate of visual associative long-term memory in the primate temporal cortex. *Nature* **335**, 817-820.
- Miyashita, Y. (1993) Inferior temporal cortex: where visual perception meets memory. *Annu. Rev. Neurosci.* **16**, 245-263.
- Murray, E.A., Gaffan, D., & Mishkin, M. (1993) Neural substrates of visual stimulus-stimulus association in rhesus monkeys. *J. Neurosci.* **13**, 4549-4561.
- Nakamura, K., Mikami, A., & Kubota, K. (1992) Activity of single neurons in the monkey amygdala during performance of a visual discrimination task. *J. Neurophysiol.* **67**, 1447-1463.
- Naya, Y., Sakai, K., & Miyashita, Y. (1996) Activity of primate inferotemporal neurons related to a sought target in pair-association task. *Proc. Natl. Acad. Sci. U.S.A.* **93**, 2664-2669.
- Naya, Y.* , Yoshida, M. *, & Miyashita, Y. (2001) Backward spreading of memory-retrieval signal in the primate temporal cortex. *Science* **291**, 661-664. (*, These authors contributed equally to this work.)
- Naya, Y., Yoshida, M., & Miyashita, Y. (2003) Forward Processing of Long-Term

- Associative Memory in Monkey Inferotemporal Cortex. *J. Neurosci.*, **23**, 2861-2871.
- Nishijo, H., Ono, T., & Nishino, H. (1988) Topographic distribution of modality-specific amygdalar neurons in alert monkey. *J. Neurosci.* **8**, 3556-3569.
- Sakai, K., & Miyashita, Y. (1991) Neural organization for the long-term memory of paired associates. *Nature* **354**, 152-155.
- Saleem, K.S., & Tanaka, K. (1996) Divergent projections from the anterior inferotemporal area TE to the perirhinal and entorhinal cortices in the macaque monkey. *J. Neurosci.* **16**, 4757-4775.
- Salin, P.A., Girard, P., Kennedy, H., & Bullier, J. (1992) Visuotopic organization of corticocortical connections in the visual system of the cat. *J. Comp. Neurol.* **320**, 415-434.
- Squire, L.R., & Zora-Morgan, S. (1991) The medial temporal-lobe memory system. *Science* **253**, 1380-1386.
- Sur, M., & Leamey, C.A. (2001) Development and plasticity of cortical areas and networks. *Nat. Rev. Neurosci.* **2**, 251-262.
- Suzuki, W.A., & Amaral, D.G (1994) Perirhinal and parahippocampal cortices of the macaque monkey – cortical afferents. *J. Comp. Neurol.* **350**, 497-533.
- Tamura, H., & Tanaka, K. (2001) Visual response properties of cells in the ventral and dorsal parts of the macaque inferotemporal cortex. *Cereb. Cortex* **11**, 384-399.
- Tokuyama, W., Okuno, H., Hashimoto, T., Li, Y.X., & Miyashita, Y. (2000) BDNF upregulation during declarative memory formation in monkey inferior temporal cortex. *Nature Neurosci.* **3**, 1134-1142.

- Yoshida, M., Naya, Y., Ito, A., Shibata, S., & Miyashita, Y. (1999a) Divergence and Convergence of area TE -> area 36 pathway in Macaque Inferotemporal Cortex. *Jpn. J. Physiol. Suppl.*
- Yoshida, M., Naya, Y., Ito, A., Shibata, S., & Miyashita, Y. (1999b) A triple injection study of the pathway from area TE to area 36 of macaque monkey. *Soc. Neurosci. Abst.* 29
- Yoshida, M., Naya, Y., Ito, A., Shibata, S., & Miyashita, Y. (2000) A combined study of tract-tracing and electrophysiological mapping in area TE and area 36 of macaque monkey. *Soc. Neurosci. Abst.* 30: 106
- Yoshida, M., Naya, Y., Ito, A., Shibata, S., & Miyashita, Y. (2001a) A Combined Single-Unit and Tract-Tracing Study Revealed Target-Specific Connectivity from Area TEav to Area 36 in the Inferotemporal Cortex of Macaque Monkeys. *Jpn. J. Physiol. Suppl.*
- Yoshida, M., Naya, Y., Ito, A., Shibata, S., & Miyashita, Y. (2001b) A combined single-unit and tract-tracing study revealed connectivity between functional domains of area TE and area 36 of macaque temporal lobe. *Soc. Neurosci. Abst.* 31: 399
- Yoshida, M.^{*}, Naya, Y.^{*}, and Miyashita, Y. (2003) Anatomical organization of forward fiber projections from area TE to perirhinal neurons representing visual long-term memory in monkeys. *Proc. Natl. Acad. Sci. U.S.A.*, **100**, 4257-4262. (*, These authors contributed equally to this work.)
- Zola-Morgan, S., Squire, L.R., Amaral, D.G., & Suzuki, W.A. (1989) Lesions of perirhinal and parahippocampal cortex that spare the amygdala and hippocampal formation produce severe memory impairment. *J. Neurosci.* **9**, 4355-4370.